~1% of the objects in the scattered disk remain after 4 billion years, and that 6×10^8 comets are currently required. Thus, we require an initial population of only 6×10^{10} comets [~0.4 Earth masses (*23*)] on Neptune-encountering orbits. Because planet formation is unlikely to have been 100% efficient, the original disk could have resulted from the scattering of even a small fraction of the tens of Earth masses of cometary material that must have populated the outer solar system in order to form Uranus and Neptune.

REFERENCES AND NOTES

1. See H. F. Levison in *Completing the Inventory of the Solar System*, T. W. Rettig and J. M. Hahn, Eds. (Astronomical Society of the Pacific, San Francisco, 1996), p. 173. To be precise, a JFC is defined to have a Tisserand parameter, T, with respect to Jupiter of between 2 and 3. The encounter velocity is $v_j\sqrt{3-T}$, where v_j is the mean orbital velocity of Jupiter around the sun. JFCs typically have semi-major axes < 7 AU and perihelion distances less than 3 AU. Their mean inclination is ~10°.
2. J. Fernández, *Mon. Not. R. Astron. Soc.* **192**, 481 (1980).
3. K. E. Edgeworth, *J. Br. Astron. Assoc.* **53**, 181 (1943); *Mon. Not. R. Astron. Soc.* **109**, 600 (1949); G. Kuiper, in *Astrophysics: A Topical Symposium*, J. A. Hynek, Ed. (McGraw Hill, New York, 1951), p. 357.
4. M. J. Duncan, T. R. Quinn, S. Tremaine, *Astrophys. J.* **328**, L69 (1988); T. R. Quinn, S. Tremaine, M. J. Duncan, *ibid.* **355**, 667 (1990).
5. H. F. Levison and M. J. Duncan, *Astrophys. J.* **406**, L35 (1993); M. Holman and J. Wisdom, *Astron. J.* **105**, 1987 (1993); M. J. Duncan, H. F. Levison, M. S. Budd, *ibid.* **110**, 3073 (1995).
6. H. F. Levison and M. J. Duncan, *Icarus*, in press.
7. A Kolmogorov-Smirnov test shows that the probability that the two distributions are derived from the same parent distribution is greater than 90% if the particles have physical lifetimes of ~12,000 years.
8. J. A. Fernandez and W.-H. Ip, *Icarus* **54**, 377 (1983); M. V. Torbett, *Astron. J.* **98**, 1477 (1989).
9. Once SIOs are perturbed inward by Neptune, they are dynamically indistinguishable from KBOs because an SIO and a KBO will have similar Tisserand parameters with respect to Neptune. Thus, it is not possible to distinguish between the two sources based on the dynamics of the JFCs alone. However, M. F. A'Hearn *et al.* [*Icarus* **118**, 223 (1995)] have shown that there are two distinct populations of JFCs based on chemical abundances. Perhaps this indicates that there are two different source for the JFCs.
10. This behavior can also be seen in figure 5 of M. Holman and J. Wisdom, *Astron. J.* **105**, 1987 (1993). This earlier work demonstrates that the basic processes of temporary capture into mean motion resonance are not dependent upon the details of how we integrated close encounters in our simulation.
11. To first order, the orbit of a particle has two precessions associated with it. The first is the precession of the location where the orbit crosses the plane of the solar system (known as node-crossing). The second is the precession of the longitude of perihelion. The Kozai resonance [Y. Kozai, *Astron. J.* **67**, 591 (1962)] occurs when the rate of these two precessions are the same. When a particle is in the Kozai resonance, it generally will not cross the plane of the solar system when it is at perihelion. Thus, particles with perihelion distances near Neptune will be protected from encounters with Neptune by the Kozai resonance.
12. We define a "visible" JFC as one with a perihelion distance < 2.5 AU. See (*6*) above for more details.
13. The observed population of JFCs suffers from observational biases, particularly with regard to a comet's perihelion distance and absolute magnitude. To perform a comparison between the results of our simulations and observations, we must correct for observational selection effects. A complete analysis is beyond the scope of this paper and we adopt the results in (*6*).
14. R. Malhotra, *Astron. J.* **110**, 420, (1995).
15. Currently, 42 trans-neptunian objects have been discovered from the ground (see http://cfa-www.harvard.edu/cfa/ps/lists/TNOs.html for a current list). Of those, 23 have been observed long enough and often enough to have well-determined orbits. The rest have not been observed enough, either because they are recently discovered or have been lost. Of those with good orbits, we categorize all but 1996 RQ_{20} and 1996 TL_{66} as KBOs.
16. E. Helin, D. Brown, D. Rabinowitz, *Minor Planet Electron. Circ. B19* (1997).
17. C. Trujillo *et al.*, *ibid. B18* (1997); J. Luu *et al.*, *Nature*, **387**, 573 (1997).
18. D. Jewitt, J. Luu, J. Chen, *Astron. J.* **112**, 1225, (1997).
19. This estimate is uncertain because the survey that found 1996 TL_{66} (*17*) had a different limiting magnitude and covered a different area of the sky than (*18*)
20. For a review, see P. R. Weissman and H. F. Levison, in *Pluto*, D. J. Tholen and S. A. Stern, Eds. (University of Arizona Press, Tucson, in press).
21. J. A. Fernandez and W.-H. Ip, *Icarus* **58**, 109 (1984).
22. S. A. Stern, *Astron. J.* **110**, 856 (1995); D. R. Davis and P. Farinella, *Icarus* **125**, 50 (1997).
23. We adopt an average mass of a comet of 6×10^{-12} Earth masses [P. R. Weissman, *Geol. Soc. Am. Spec. Pap.* **247**, 263 (1990)]. This value is uncertain, because the size distribution is poorly determined.

24. We are grateful to S. Tremaine, who motivated this line of inquiry. We also thank L. Dones, B. Marsden, A. Stern, B. Gladman, M. Holman, W. Merline, and P. Weissman for comments on this manuscript. H.F.L. acknowledges grants provided by the NASA Origins of Solar Systems and Planetary Geology and Geophysics Programs. M.J.D. is grateful for the continuing financial support of the Natural Science and Engineering Research Council of Canada and for financial support for work done in the U.S. from NASA Planetary Geology and Geophysics Programs. We also acknowledge funding for our computer equipment from the National Science Foundation and the Southwest Research Institute.

3 February 1997; accepted 16 May 1997

Paleobotanical Evidence for High Altitudes in Nevada During the Miocene

Jack A. Wolfe,* Howard E. Schorn, Chris E. Forest, Peter Molnar

Leaf physiognomy provides estimates of environmental parameters, including mean annual enthalpy, which is a thermodynamic parameter of the atmosphere that varies with altitude. Analyses of 12 mid-Miocene floras from western Nevada indicate that this part of the Basin and Range Province stood ~3 kilometers above sea level at 15 to 16 million years ago, which is 1 to 1.5 kilometers higher than its present altitude. Much, if not all, of the collapse to present-day altitudes seems to have been achieved by ~13 million years ago. The crust in much of this area has been extended and thinned throughout the past 40 to 50 million years, and the isostatic balance of a thinning crust requires subsidence, not uplift as suggested by previous paleobotanical work.

Terrestrial plants are generally regarded as highly responsive to environmental changes, and thus fossil plants offer one of the best methods for inferring paleoenvironmental parameters (*1*). In one approach, the environmental tolerances of a fossil species were assumed to be the same as those of its nearest living relative. Because in this method it was assumed that plants do not evolve by adapting to different environments (*2*), conclusions based on this method must—to varying degrees—be doubtful. Paleobotanical data using this nearest living relative method have been interpreted to indicate that most of the Basin and Range Province of Nevada was at low altitudes (<1 km) until <5 million years ago (Ma), when uplift is inferred to have started, which resulted in the ~1- to 1.5-km present-day mean altitudes of the basins (*3*). These estimates have been used as boundary conditions in numerical models of global climate during the Cenozoic, and it has been suggested that recent uplift helped initiate late Cenozoic glaciation (*4*). A second paleobotanical method relates the general physiognomy of plants to the environment, a relation that has generally been assumed to be valid, both today and in the past (*1*). In particular, gross physical aspects of leaves, including outlines, shapes, and sizes that can be readily observed on fossilized leaves, can be observed to change along present-day environmental gradients (*5*).

To calibrate changes in foliar physiognomy with changes in environmental parameters, leaves of at least 20 species of woody dicotyledons were collected close to meteorological recording stations (*5*), primarily in North America and the Caribbean region from latitudes 18°N to 62°N. Included in the sampling was vegetation ranging

J. A. Wolfe, Department of Geosciences, University of Arizona, Tucson, AZ 85721, USA.
H. E. Schorn, Museum of Paleontology, University of California, Berkeley, CA 94720, USA.
C. E. Forest and P. Molnar, Department of Earth, Atmospheric, and Planetary Sciences, Massachusetts Institute of Technology, Cambridge, MA 02139, USA.

*To whom correspondence should be addressed. E-mail: jwolfe@geo.arizona.edu

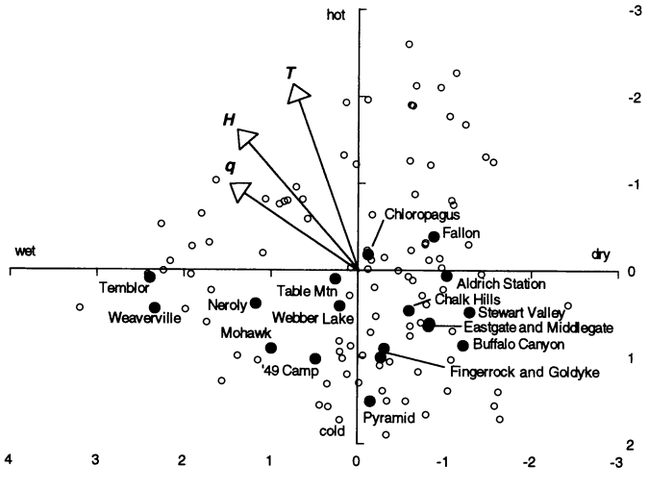

Fig. 1. Plot of the canonical correspondence analysis of environmental factors (arrows), modern samples (open circles), and fossil leaf assemblages (solid circles). Axis 1 (which is shown as vertical here), which explains ~50% of the physiognomic variation, represents temperature factors; whereas axis 2, which explains ~20% of the physiognomic variation, represents water stress. The length of the environmental vector approximates the relative significance of the environmental factor in explaining variation; enthalpy, which varies relative to altitude, is almost as significant as mean annual temperature. Other environmental factors included in the analysis but not shown here are the cold-month and warm-month mean temperatures, growing season length, precipitation during the three consecutive driest months and three consecutive wettest months during the growing season, mean growing season and mean annual precipitation, and relative humidity, all of which had shorter vectors than *T* and *H*. The modern samples analyzed exclude the subalpine samples.

Fig. 2. Map of part of California and Nevada showing the present-day topography and the Miocene fossil sites (+) that produced the collections of leaves analyzed in this report. Numbers coordinate with those in parentheses after the assemblage names in Table 1. Not shown is Molalla, which is about 50 km southeast of Portland, Oregon, on the eastern side of the Willamette Valley.

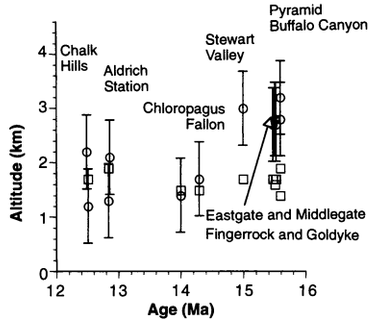

Fig. 3. Paleoaltitudinal estimates for middle Miocene leaf assemblages of western Nevada (circles) versus time. The altitude estimates for assemblages from ~15 to 16 Ma are consistently higher than present-day altitudes (denoted by squares), whereas late middle Miocene (12 to 14 Ma) assemblages have estimates that are close to present-day altitudes.

from desert to wet tropical forest to boreal forest. Physiognomic character states determined or measured for all species in the samples were then analyzed in a multivariate context. In the Climate-Leaf Analysis Multivariate Program (CLAMP), we used canonical correspondence analysis (*6*, *7*), a multivariate ordination method that is widely used in ecology (*8*) to rank samples simultaneously relative to several environmental factors (such as temperature and precipitation values) by partial constraint of the ordination axes by supplied environmental data. Because leaf physiognomy character states have typically nonlinear relations to environmental parameters (*5*), canonical correspondence analysis, which was developed to analyze nonlinear relations, is preferred to methods that assume linear relations (such as multiple regression analysis).

Among the environmental parameters that can be inferred from leaf physiognomy, we concentrated on mean annual temperature, specific humidity, and enthalpy (Fig. 1). Forest *et al.* (*9*) have shown that mean annual values of moist static energy, a thermodynamically conserved variable in the atmosphere, are approximately zonally invariant. The moist static energy h of an air parcel consists of three terms that quantify the total energy content (per unit of mass) of the air parcel (the negligibly small kinetic energy is excluded):

$$h = c_pT + L_vq + gZ = H + gZ$$

where c_p is the specific heat capacity of moist air at constant pressure, T is the absolute temperature, L_v is the latent heat of vaporization, q is the specific humidity, g is the gravitational acceleration, Z is height, and H ($= c_pT + L_vq$) is enthalpy. With the assumption that moist static energy is zonally invariant, the difference between two estimates of mean annual enthalpy for sites at similar paleolatitudes should yield an estimate of their difference in potential energy, gZ.

Some error is introduced because moist static energy varies with longitude; this error (σ_h) has been estimated (*9*, *10*) to be 4.5 kJ kg^{-1}. Additional error is introduced because the enthalpy predicted for sites in the CLAMP database differs from observed or calculated enthalpy. In canonical correspondence analysis, the standard error for the predicted enthalpy (σ_H) is 4.2 kJ kg^{-1}. When the standard error is applied to two coeval sites, the combination of the two errors produces a standard error in the estimated difference in altitude of ~760 m

$$\sigma_Z = \sqrt{\frac{2\sigma_H^2 + \sigma_h^2}{g^2}} = 760 \text{ m}$$

In a previous analysis that estimated altitude for a late Eocene (~35 Ma) flora in Colorado, Forest *et al.* (*9*) used principal components analysis, which assumes linearity, to derive direct estimates of enthalpy and of mean annual temperature (T) and specific humidity (q) for samples then composing the CLAMP database (*11*). Canonical correspondence analysis corroborates that H, T, and q can be estimated from leaf physiognomy, and, although q is not linearly independent of T, their dependence is not great (Fig. 1).

The floras included in our analyses occur in an area bounded by the Pacific Ocean and almost 118°W longitude and by 36°N and 42°N latitude, except for one flora at ~45°N (Fig. 2). As shown in Table 1, the estimates of enthalpy from CLAMP for assemblages from rocks deposited 15 to 16 Ma in the Basin and Range of western Nevada imply that paleoaltitudes were 2.9 to 3.2 km. The Fallon and Chloropagus assemblages imply that paleoaltitudes were close to present altitudes and thus that the collapse might have occurred between 14 and 15 Ma; the size of these assemblages is, however, small, and thus interpretations are uncertain (*12*). The Chalk Hills and Aldrich Station assemblages indicate that by ~12.5 to 13 Ma, western Nevada stood at about its present altitude (Fig. 3). The trend to increasing temperature shown by the Nevada mid-Miocene floras is counter to the observations from oxygen isotope data in

the marine record that global climates generally cooled between 15 and 10 Ma (*13*). These data also show some moderate reversals in declining temperature during the 13 to 15 Ma interval, so we offer alternative estimates of heights for the Chalk Hills and Aldrich Station, one set using the 10.5- to 11.0-Ma Neroly leaf assemblage, which formed near sea level, and the second set using the 13.1-Ma Molalla assemblage near Portland, Oregon, which was also at a low altitude. Either set places the Miocene altitudes of the Chalk Hills and Aldrich Station at no more than 400 m above or 600 m below their present altitudes.

The Weaverville assemblage (~14 to 18 Ma) is based on localities from three separate basins of low altitude, which are assumed to have once been in the same depositional basin (*14*). The CLAMP analyses suggest that the altitude of the basin has changed little, if any, since deposition. Similarly, the Mohawk, Webber Lake (both ~14 to 18 Ma), and Table Mountain (10.5 Ma) assemblages from the Sierra Nevada of northern California all have paleoaltitudinal estimates within 700 m of the present-day altitudes at the fossil localities. Since 14 to 18 Ma, the Sierra Nevada may have been no more than the western flank of the high plateau that constituted western Nevada; our data and interpretations are consistent with the model of uplift for the Sierra Nevada proposed by Small and Anderson (*15*).

The estimates of mid-Miocene altitudes of 2.9 to 3.2 km are somewhat lower than the estimates of 3 to 4 km (*16*), based on estimates of T derived from CLAMP and present-day terrestrial lapse rates [(TLR) which is the gradient of surface temperatures dT_s/dZ measured at different surface heights, Z]. The degree to which modern TLR applies to the past is not clear (*9, 10*). Our independent estimates of T and elevations imply that the mid-Miocene TLR was 2.0° to 3.3°C km^{-1}, which is about half that of the average modern worldwide TLR of 5.5°C km^{-1} (*3*) but is comparable to the present-day empirically estimated value for much of mid-latitude western North America (*17*).

Paleobotanical evidence supports the hypothesis that Mesozoic thrust faulting and crustal thickening built a high terrain in what is now the Basin and Range Province (*18, 19*). By analogy with the Andes and the Tibetan Plateau, altitudes in Nevada could have been even higher than ~3 km before 16 Ma. Our results imply decreasing altitudes at about the time that most Basin and Range–style faulting began in the Great Basin. Thus, late Cenozoic uplift of Nevada (*3*) does not appear to have occurred. The drop in elevations reported here concurs with similar paleobotanical arguments for high latest Eocene elevations in the Rocky Mountains of Colorado based on nearest living relative and general physiognomic arguments (*20*) and on multivariate analysis of leaf physiognomy (*21*). Molnar and England (*22*) also have suggested that many previous estimates of paleoaltitudes for the early and middle Tertiary of western North America were much too low. Geophysical observations combined with theoretical considerations of the region to the south of our study area suggested high altitudes at ~20 Ma and a subsequent collapse (*23*); an increasing body of data and interpretations argue for

Table 1. Environmental estimates for some California, Oregon, and Nevada Miocene fossil leaf assemblages (*25*). Ages given as decimals are radiometric ages (*26*), except for Temblor and Neroly, whose ages are based on a marine time scale. Alternative 1 uses Neroly as the low-altitude time equivalent. Alternative 2 uses Molalla in Willamette Valley as the low-altitude time equivalent. No., number; Paleolat., paleolatitude; Alt., altitude; Est., estimated. T, mean annual temperature; standard error, 1.3°C. H, enthalpy; standard error, 4.2 kJ kg^{-1}. The numbers in parentheses refer to locations in Fig. 2. Dashes indicate that altitude was at (or near) sea level.

Assemblage	No. of species	Paleolat. (°N)	Present alt. (km)	Age (Ma)	Estimates from CLAMP		Est. alt.* (km)	Change in alt.† (km)	Est. TLR‡ (°C km^{-1})	Present TLR (°C km^{-1})
					T (°C)	H (kJ kg^{-1})				
Early middle Miocene (~15 to 16 Ma)										
Temblor§ (1)	30	39.3	0.5	15.0–15.5	18.3	325.5	0	+0.5	–	–
Weaverville§ (2)	33	43.7	0.4–0.7	~14–18	16.1	321.1	~0.1	+0.3–0.6	–	–
'49 Camp‖ (3)	25	44.5	1.5	15.5–16.0	10.2	301.8	2.1	−0.6	2.6	3.3
Pyramid‖ (4)	26	42.7	1.4	15.6	7.5	294.2	2.8	−1.4	3.2	1.9
Buffalo Canyon‖ (5)	26	42.2	1.9	15.6	8.7	292.7	3.2	−1.3	2.5	1.8
Eastgate‖ (6)	25	42.3	1.7	15.5	10.3	296.9	2.7	−1.0	2.4	1.7
Middlegate‖ (7)	26	42.3	1.6	15.5	10.2	296.7	2.8	−1.2	2.3	1.7
Stewart Valley‖ (8)	36	41.3	1.7	14.5–15.0	10.2	295.1	3.0	−1.2	2.3	1.7
Fingerrock‖ (9)	30	41.3	1.7	15.5	9.3	297.2	2.8	−1.1	2.8	1.7
Goldyke‖ (10)	32	41.3	1.7	15.5	9.7	297.7	2.7	−1.0	2.8	1.7
Middle middle Miocene (~14 Ma)										
Weaverville§ (2)	33	43.7	0.4–0.7	~14–18	16.1	321.1	~0.1	0.3–0.6	–	–
Mohawk§ (11)	19	42.8	1.3	~14–18	11.5	306.3	1.6	−0.7	3.1	3.0
Webber Lake§ (12)	41	42.5	2.1	~14–18	12.8	305.2	1.7	+0.4	2.2	2.3
Fallon‖ (13)	15	42.5	1.5	~14	15.4	308.1	1.4	+0.1	0.9	0.6–1.7
Chloropagus‖ (14)	15	42.6	1.5	14.3	15.2	304.6	1.7	−0.2	0.7	0.6–1.7
Late middle Miocene (~10.5 to 14 Ma): alternative 1										
Neroly§ (15)	21	39.8	<0.1	10.5–11.0	14.4	312.4	0	~0	–	–
Table Mtn.§ (16)	28	39.8	0.7	10.5	14.5	308.3	0.4	+0.3	0.0	−4.0
Chalk Hills‖ (17)	20	41.5	1.7	12.5	11.3	299.4	1.2	+0.5	1.9	2.0–2.4
Aldrich Station‖ (18)	24	40.7	1.9	12.4–13.3	12.6	299.9	1.3	+0.6	1.6	1.0–1.7
Late middle Miocene (~10.5 to 14 Ma): alternative 2										
Molalla¶	25	47.3	~0.1	13.1	14.8	316.6	0	~0	–	–
Chalk Hills‖ (17)	20	41.5	1.7	12.5	11.3	299.4	2.1	−0.4	3.1	2.0–2.4
Aldrich Station‖ (18)	24	40.7	1.9	12.4–13.3	12.6	299.9	2.1	−0.2	2.7	1.0–1.7

*Estimated altitudes are derived by division of enthalpy differences between coastal and inland assemblages by 9.8 and assumption of a poleward decline of 0.6 kJ kg^{-1} (1° latitude)$^{-1}$ (*10*). †Negative value, loss; positive value, gain. ‡Estimated TLRs are derived from differences in T between coastal and interior assemblages, if one assumes a poleward decline in T of 0.5°C (1° latitude)$^{-1}$; this value is the difference in T between near-coastal Alaskan and western conterminous United States Miocene leaf assemblages and is also approximately the present-day mean annual latitudinal temperature gradient. §These sites are in California. ‖These sites are in Nevada. ¶This site is in Oregon.

high altitudes during the Tertiary in much of western North America (*24*). The contention that late Cenozoic uplift of mountain ranges and plateaus throughout the world was a trigger for the onset of the Ice Age (*5*) should be reevaluated.

REFERENCES AND NOTES

1. P. W. Richards, *The Tropical Rain Forest* (Cambridge Univ. Press, Cambridge, 1952); R. A. Spicer, *Trans. R. Soc. Edinburgh* **80**, 321 (1989); A. B. Herman and R. A. Spicer, *Nature* **381**, 330 (1996).
2. J. A. Wolfe and H. E. Schorn, *Paleobiology* **15**, 180 (1989).
3. D. I. Axelrod, *Univ. Calif. Publ. Geol. Sci.* **39**, 195 (1962); *ibid.* **34**, 91 (1958); *ibid.* **135**, 1 (1991); *ibid.* **137**, 1 (1992).
4. W. F. Ruddiman and J. E. Kutzbach, *J. Geophys. Res.* **94**, 409 (1989).
5. J. A. Wolfe, *Nature* **343**, 153 (1990); *U.S. Geol. Surv. Bull. 2040* (1993); *Annu. Rev. Earth Planet. Sci.* **23**, 119 (1995).
6. C. J. F. ter Braak, *Biometrics* **41**, 859 (1985); *Ecology* **67**, 1167 (1986); C. J. F. ter Braak and I. C. Prentice, *Adv. Ecol. Res.* **18**, 271 (1988).
7. The tabulations for the leaf assemblages were run with the software CANOCO. This software is available from Microcomputer Power, 111 Clover Lane, Ithaca, NY 14850.
8. H. J. B. Birks, S. M. Peglar, H. A. Austin, *An Annotated Bibliography of Canonical Correspondence Analysis and Related Constrained Ordination Methods 1986–1993* (Univ. of Bergen Botanical Institute, Bergen, Norway, 1994).
9. C. E. Forest, P. Molnar, K. A. Emanuel, *Nature* **374**, 347 (1995).
10. C. E. Forest, thesis, Massachusetts Institute of Technology (1996).
11. The database furnished earlier to Forest comprised 106 samples, including 25 that represent outliers and inliers in plots of samples on axes 1 and 2 (*5*). The elimination of these 25 samples reduced standard errors of estimates of environmental parameters and increased axis eigenvalues. Samples (including 12 from the largely deciduous vegetation of southern Sonora and Baja California) have subsequently been added to the database, which now comprises 97 samples, excluding the 25 outliers and inliers. Both the physiognomic and meteorological data sets, as well as the locality data for the new samples, can be obtained from J. A. Wolfe.
12. D. A. R. Povey, R. A. Spicer, P. C. England, *Rev. Palaeobot. Palynol.* **81**, 1 (1994).
13. B. J. Flower and J. P. Kennett, *Paleoceanography* **10**, 1095 (1995).
14. H. D. MacGinitie, *Carnegie Inst. Washington Publ.* **465**, 83 (1937).
15. E. E. Small and R. S. Anderson, *Science* **270**, 277 (1995).
16. J. A. Wolfe and H. E. Schorn, *Geol. Soc. Am. Abstr. Program* **26**, A521 (1994).
17. J. A. Wolfe, *U.S. Geol. Surv. Bull. 1964* (1992).
18. P. Molnar and W.-P. Chen, *J. Geophys. Res.* **88**, 1180 (1983); P. J. Coney and T. A. Harms, *Geology* **12**, 550 (1984).
19. P. Molnar and H. Lyon-Caen, *Geol. Soc. Am. Spec. Pap.* **218**, 179 (1988).
20. H. W. Meyer, *Palaeogeogr. Palaeoclimatol. Palaeoecol.* **99**, 71 (1992).
21. K. M. Gregory and C. G. Chase, *Geology* **20**, 581 (1992).
22. P. Molnar and P. C. England, *Nature* **346**, 29 (1990).
23. B. Wernicke *et al.*, *Science* **271**, 190 (1996).
24. R. A. Kerr, *ibid.* **275**, 1564 (1997).
25. Revisions to the taxonomy were made by Wolfe and Schorn before the analysis of some of these assemblages. Other than (*3, 14*), available sources include R. S. LaMotte, *Carnegie Inst. Washington Publ.* **455**, 57 (1936); C. Condit, *ibid.* **476**, 217 (1938); *ibid.* **553**, 57 (1944); D. I. Axelrod, *Univ. Calif. Publ. Geol. Sci.* **33**, 1 (1956); *ibid.* **129**, 1 (1985); J. A. Wolfe, *U. S. Geol. Surv. Prof. Pap. 454-N*, N1 (1964); and K. M. Renney, thesis, University of California, Davis (1969). In all instances, we examined original collections in the University of California Museum of Paleontology (Berkeley).
26. C. C. Swisher III, thesis, University of California, Berkeley (1992).

27. This work was partially supported by NSF (Atmospheric Sciences).

2 April 1997; accepted 28 April 1997

Photodissociation of $I_2^-(Ar)_n$ Clusters Studied with Anion Femtosecond Photoelectron Spectroscopy

B. Jefferys Greenblatt,* Martin T. Zanni,* Daniel M. Neumark†

Anion femtosecond photoelectron spectroscopy was used to follow the dynamics of the $I_2^-(Ar)_6$ and $I_2^-(Ar)_{20}$ clusters subsequent to photodissociation of the I_2^- chromophore. The experiments showed that photodissociation of the I_2^- moiety in $I_2^-(Ar)_6$ is complete by approximately 200 femtoseconds, just as in bare I_2^-, but also that attractive interactions between the departing anion fragment and the solvent atoms persisted for 1200 femtoseconds. Photodissociation of $I_2^-(Ar)_{20}$ results in caging of the I_2^- followed by recombination and vibrational relaxation on the excited $\tilde{A}\,^2\Pi_{g,3/2}$ and the ground $\tilde{X}\,^2\Sigma_u^+$ states; these processes are complete in 35 and 200 picoseconds, respectively.

Understanding of the potential energy surfaces governing the dynamics of elementary chemical reactions in the gas phase has grown significantly during the past 10 years, largely because of the development of new frequency- and time-resolved experimental techniques (*1*, *2*) combined with theoretical advances in quantum chemistry (*3*) and reaction dynamics (*4*). A very appealing new direction in this field is to investigate, in a systematic way, the effects of solvation on reaction dynamics. Studies of chemical reactions occurring within size-selected clusters provides an elegant means of achieving this goal, because one can monitor the changes that occur as a function of cluster size and ultimately learn how the dynamics of an elementary unimolecular or bimolecular reaction evolve as a condensed-phase environment is approached (*5*). It is particularly useful to perform such experiments on ionic clusters, for which size selection is straightforward. We recently performed a time-resolved study of the photodissociation dynamics of the I_2^- anion, using a new technique—anion femtosecond photoelectron spectroscopy (FPES) (*6*). We now apply this method to follow the dynamics that result from photodissociation of the I_2^- chromophore in the clusters $I_2^-(Ar)_6$ and $I_2^-(Ar)_{20}$. These experiments yielded time-resolved measurements of the anion-solvent interactions subsequent to photodissociation and, in the case of $I_2^-(Ar)_{20}$, provided new insight into the caging and recombination dynamics of the I_2^- moiety.

Anion FPES is a pump-probe experiment using laser pulses of ~100 fs duration in which a pump pulse photodissociates an anion (or anion chromophore in a cluster) and a probe pulse ejects an electron from the dissociating species. By measurement of the resulting photoelectron (PE) spectrum at various delay times, the experiment yields "snapshots" of the dissociation dynamics and, in particular, probes how the local environment of the excess electron evolves with time. This highly multiplexed experiment yields information on the entire photoexcited wavepacket at each delay time without having to vary the wavelength of the probe pulse; this is in contrast to most pump-probe experiments in which only an absorption of the probe pulse is monitored. Although FPES has also been applied to neutrals (*7–9*), the anion experiment is inherently mass-selective, making it especially useful in studies of size-selected clusters.

Our work here builds on the experiments of Lineberger and co-workers (*10–12*), who performed one-photon photodissociation and time-resolved pump-and-probe experiments on size-selected $I_2^-(CO_2)_n$ and $I_2^-(Ar)_n$ cluster anions, and on the time-resolved studies of neutral $I_2(Ar)_n$ clusters by Zewail and co-workers (*13*). The one-photon cluster anion experiments yielded the asymptotic daughter ion distributions as a function of initial cluster size; in particular, the relative amounts of "caged" $I_2^-(Ar)_{m1<n}$ products in which the I and I^- photofragments are trapped by the

Department of Chemistry, University of California, Berkeley, CA 94720, and Chemical Sciences Division, Lawrence Berkeley National Laboratory, Berkeley, CA 94720, USA.

*These authors contributed equally to this work.
†To whom correspondence should be addressed. E-mail: dan@radon.cchem.berkeley.edu